Magnetic bilayer-skyrmions without skyrmion Hall effect

Xichao Zhang[1], Yan Zhou[1,2],* and Motohiko Ezawa[3]†
[1]*Department of Physics, University of Hong Kong, Hong Kong, China*
[2]*Center of Theoretical and Computational Physics, University of Hong Kong, Hong Kong, China and*
[3]*Department of Applied Physics, University of Tokyo, Hongo 7-3-1, 113-8656, Japan*

Arising from emergent electromagnetic field of magnetic skyrmions due to their nontrivial topology, the skyrmion Hall effect might be a roadblock for practical applications since any longitudinal motions of skyrmions in nanotrack is accompanied by a transverse motion. A direct consequence of such an effect is easy destruction of skyrmions at the nanotrack edges during their fast motions along the nanotrack, despite their topological protection. Here we propose an entirely novel solution of completely inhibiting such skyrmion Hall effect without affecting its topological properties based on a antiferromagnetic-coupling bilayer system. We show that a pair of magnetic skyrmions can be nucleated in such a bilayer system through vertical current injection or converted from a current-driven domain-wall pair. Once nucleated, the skyrmion pair can be displaced through current-induced spin torque either from a vertical injected current or in-plane current. The skyrmion Hall effect is completely suppressed due to the cancellation of back-action forces acting on each individual skyrmion, resulting in a straight and fast motion of skyrmions along the current direction. This proposal will be of fundamental interests by introducing the bilayer degree of freedom into the system. Moreover, it provides an easy way to engineer the transport properties of the skyrmionic devices to achieve desired performance, making it highly promising for practical applications such as ultradense memory and information-processing devices based on skyrmions.

Since the first experimental observations of magnetic skyrmion lattices in bulk non-centrosymmetric magnets[1,2] and films[3], there has been tremendous interest in these topologically protected spin configurations with a quantized topological number[4,5]. However, the creation and transmission of isolated magnetic skyrmion in magnetic thin films are required for any practical applications such as encoding information in individual skyrmion to allow entirely novel devices and circuitry[5–11]. Significant efforts and progress have been made towards realizing such ultrathin film based on perpendicularly magnetized magnetic layer|heavy metal structure to host a rich variety of chiral spin textures including skyrmions[12,13]. The strong spin orbit coupling at the interfaces between the magnetic layer with perpendicular magnetic anisotropy (PMA) and the underlying heavy metal layer provides a sizeable Dzyaloshinsky-Moriya interaction (DMI) to stabilize skyrmions[5,14–17].

To move a skyrmion in nanotrack for information-processing applications, a convenient and efficient way is by means of spin current which can transfer the angular momentum from itinerant conduction electrons to the magnetic moments of the skyrmion[18,19]. However, one major roadblock to the manipulation and transmission of skyrmions in nanotrack is the skyrmion Hall effect, *i.e.*, skyrmions exhibit the Hall effect driven by spin currents due to the presence of the Magnus force which in turn originates from its nontrivial topology[4]. Thus a skyrmion will not move parallel with the direction of the current. Instead it will gain a transverse velocity with a magnitude proportional to the spin current density which displaces the skyrmion towards the edge of the nanotrack. Therefore a skyrmion will be easily destroyed for a distance of much less than 1μm for a nanotrack made of typical magnetic layer|heavy metal system[18–20].

Since both the skyrmion Hall effect and its topological protection arise from the same mechanism, *i.e.*, its nontrivial topological number of ± 1, it seems to be impossible to inhibit the skyrmion Hall effect without breaking its topological protection. In this work, we propose a novel solution of two perpendicularly magnetized sublayers strongly coupled via the antiferromagnetic (AFM) exchange interaction with a heavy metal layer beneath the bottom magnetic layer[21] (Fig.1a, b, c). When a skyrmion is created in one of the sublayers, another skyrmion is simultaneously created in the other sublayer under certain conditions. We refer to such a pair of magnetic skyrmions as a magnetic bilayer-skyrmion (Fig.1d, e). Moreover, we show a bilayer-skyrmion can be displaced over arbitrarily long distances driven by spin currents without touching the edges due to the absence of the skyrmion Hall effect, which is distinct from a skyrmion in the monolayer thin-film structure. In addition to address the above-mentioned dilemma, bilayer-skyrmions have many distinct characteristics from conventional skyrmions in monolayer thin film, which allow for versatile and multifunctional ultradense and ultrafast information processing and logic applications.

These features are true for both the current-in-plane (CIP) and current-perpendicular-to-plane (CPP) cases. The CIP implementation has been extensively studied in the past ten years for displacing domain walls or switching magnetization. Recently, the spin Hall effect has been demonstrated to be a more efficient means of manipulating magnetization. The current for the CIP case is along the nanowire axial direction. By contrast, the spin current is perpendicular to the heavy metal/ferromagnetic interface for the CPP case. In our nomenclature for CPP, the spin current is perpendicular-to-film plane whereas the charge current can be either in the film plane (such as the spin Hall effect scenario) or perpendicular to the film plane (such as the perpendicular MRAM where a perpendicularly magnetized polarizer is incorporated). The CPP scheme has been proven to be much more efficient to move the domain wall or skyrmion than the CIP method[6,14,18,19].

In this work, we first describe the nucleation process of an

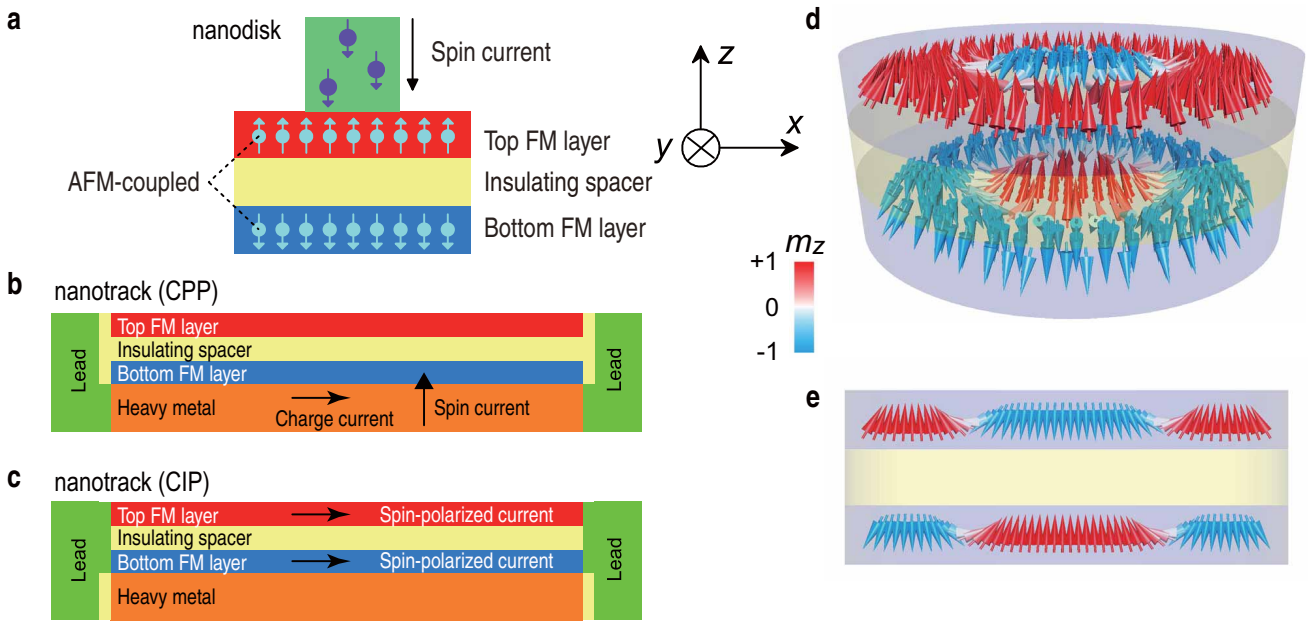

FIG. 1: **Schematics of the bilayer nanodisk, nanotrack and the bilayer-skyrmion. a**, The bilayer nanodisk for the creation of skyrmions, of which the diameter is 100 nm. The spin current (polarized along $-z$) is injected into the top layer in the central circle region with a diameter of 40 nm. **b**, The bilayer nanotrack (500 nm $\times$ 50 nm $\times$ 3 nm) for the motion of skyrmion driven by current perpendicular to the plane (CPP). The charge current flows through the heavy metal along the x-direction, which leads to the generation of spin current (polarized along $+y$) perpendicularly injected to the bottom layer due to the spin Hall effect. The skyrmion in the bottom layer is driven by the spin current, while the skyrmion in the top layer moves remotely due to the interlayer exchange coupling. **c**, The bilayer nanotrack (500 nm $\times$ 50 nm $\times$ 3 nm) for the motion of skyrmion driven by in-plane current (CIP). The electrons flow towards the right in both the top and bottom layers, *i.e.*, the charge currents flow along the -x-direction. The skyrmions in both the top and bottom layers are driven by the spin current. In all models, the thickness of both the top ferromagnetic (FM) layer, the bottom FM layer and the insulating spacer are equal to 1 nm. The top layer and bottom layer is antiferromagnetically exchange-coupled, where the initial state of the top layer is almost spin-up (pointing along +z) and that of bottom layer is almost spin-down (pointing along -z). **d**, Illustration of the bilayer-skyrmion in a nanodisk, which is a set of antiferromagnetically exchange-coupled skyrmions. **e**, Sideview of the bilayer-skyrmion along the diameter of **d**. The color scale represents the out-of-plane component of the magnetization, which is used throughout this paper.

isolated skyrmion within the top layer by utilizing the CPP injection into a disk composed of two AFM-coupled magnetic sublayers. Owing to the interlayer AFM exchange coupling, another skyrmion will automatically emerge in the bottom layer. In so doing we explore various properties of a bilayer-skyrmion. Furthermore, we move a bilayer-skyrmion in the nanotracks either by the CPP or CIP. We also study the generation of a domain-wall (DW) pair and the conversion process from a DW pair to a skyrmion in the bilayer nanotracks.

Bilayer System coupled with AFM interaction

Hamiltonian. We investigate the bilayer system where the top and bottom ferromagnetic (FM) layers are coupled antiferromagnetically by the exchange interaction, as illustrated in Fig.1a. The Hamiltonian for each layer reads

$$H_\tau = -A_{\text{intra}} \sum_{\langle i,j \rangle} \boldsymbol{m}_i^\tau \cdot \boldsymbol{m}_j^\tau + \sum_{\langle i,j \rangle} \boldsymbol{D} \cdot (\boldsymbol{m}_i^\tau \times \boldsymbol{m}_j^\tau) + K \sum_i [1 - (m_i^{\tau,z})^2] + H_{\text{DDI}}, \quad (1)$$

where τ is the layer index (τ =T, B), $\boldsymbol{m}_i^\tau$ represents the local magnetic moment orientation normalized as $|\boldsymbol{m}_i^\tau| = 1$ at the site i, and $\langle i,j \rangle$ runs over all the nearest neighbor sites in each layer. The first term represents the FM exchange interaction with the FM exchange stiffness A_{intra}. The second term represents the DMI with the DMI vector $\boldsymbol{D}$. The third term represents the PMA with the anisotropic constant K. H_{DDI} represents the dipole-dipole interaction. There exists an AFM coupling between the top and bottom layers,

$$H_{\text{inter}} = -A_{\text{inter}} \sum_i \boldsymbol{m}_i^{\text{T}} \cdot \boldsymbol{m}_i^{\text{B}}. \quad (2)$$

The sign of A_{inter} is negative reflecting that the interlayer interaction is antiferromagnetic. We assume that the spins in the top layer are pointing upward. Then the spins in the bottom layer are pointing downward due to the interlayer AFM couplings.

Topological Number. The classical field $\boldsymbol{m}^\tau(\boldsymbol{x})$ is introduced for the spin texture in the FM system by considering the zero limit of the the lattice constant, $a \to 0$. The ground-state spin textures are $\boldsymbol{m}^{\text{T}} = (0,0,1)$ and $\boldsymbol{m}^{\text{B}} = (0,0,-1)$. A magnetic skyrmion is a spin texture which has a quantized topological number. Spins swirl continuously around the core and approach the ground-state value asymptotically.

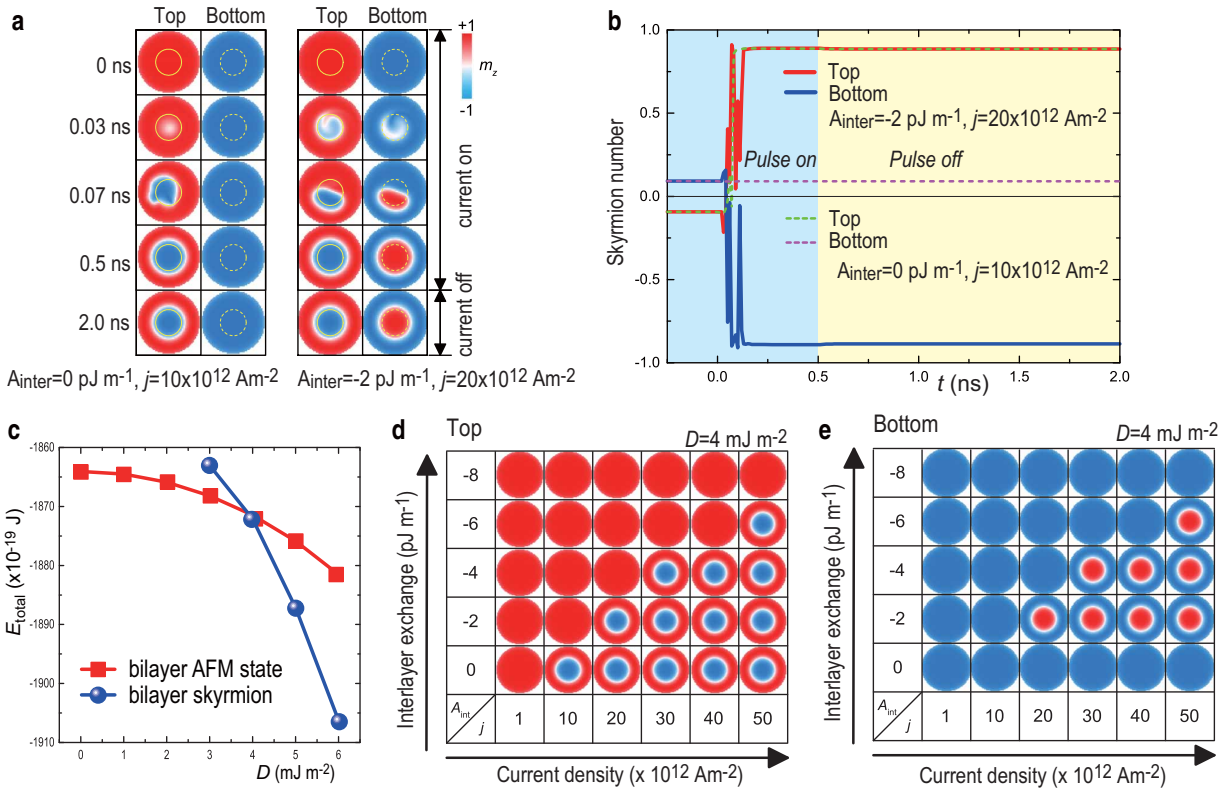

FIG. 2: **Creation of skyrmions in the bilayer nanodisk and time evolution of the skyrmion number. a**, Injection of skyrmions in the bilayer nanodisk ($D = 4$ mJ m^{-2}) with/without interlayer AFM exchange coupling. A 0.5-ns-long spin current ($P = 0.4$) is injected into the top layer (denoted by solid yellow circles), followed by a 1.5-ns-long relaxation. The interlayer exchange constant $A_{\rm inter}$ is set as 0 or -2 pJ m^{-1}, whereas the corresponding interface exchange constant σ equals to 0 or -2 mJ m^{-2} (see Supplementary Movies 1-2). **b**, The time evolution of the skyrmion number of the top and bottom layers in the nucleation process of skyrmions corresponding to **a**. **c**, Total micromagnetic energy $E_{\rm total}$ (including the intralayer exchange, interlayer exchange, dipolar, anisotropy and DMI energy) for a bilayer-skyrmion and the AFM-coupled ground state as a function of the DMI constant D. Relaxed state of (**d**) the top layer and (**e**) the bottom layer after the injection of a 0.5-ns-long spin current for various current density j and interlayer exchange constant $A_{\rm inter}$.

The skyrmion is characterized by the topological number Q_τ in each layer,

$$Q_\tau = -\frac{1}{4\pi}\int d^2x \boldsymbol{m}^\tau(\boldsymbol{x})\cdot(\partial_x \boldsymbol{m}^\tau(\boldsymbol{x})\times\partial_y \boldsymbol{m}^\tau(\boldsymbol{x}))\,. \quad (3)$$

We obtain $Q_\tau = \pm 1$ for a skyrmion in a sufficiently large area. We also call Q_τ the skyrmion number. Even if the skyrmion spin texture is deformed, its skyrmion number does not change, as far as the boundary condition is not modified. It can be neither destroyed nor separated into pieces, *i.e.*, a skyrmion is topologically protected.

The spins in the top and bottom layers are tightly bounded due to the AFM coupling. Accordingly, if one skyrmion is created in the top layer, a second skyrmion is also created in the bottom layer (Fig.2a) simultaneously. The topological number of the bottom layer is opposite to that of the top layer since all the spins are inverted, $Q_{\rm B} = -Q_{\rm T}$. See Fig.2b how these topological numbers evolve after the creation of a skyrmion in the top layer.

Excitation Energy. We may determine numerically the spin profile of each skyrmion and estimate the excitation energy based on the Hamiltonian $H_{\rm total} = H_{\rm T} + H_{\rm B} + H_{\rm inter}$. We compared the energy of one bilayer-skyrmion state and the energy of the homogeneous state in Fig.2c as a function of the DMI. Similar result is obtained for any value of the interlayer AFM coupling strength. This is because the spin directions between the top and bottom layers are always opposite.

The energy of the bilayer-skyrmion becomes lower than that of the uniform ground state for $D \gtrsim 4$ mJ m^{-2}, which is the threshold value. Consequently, the bilayer-skyrmion excitation is energetically favorable when the DMI strength is larger than the threshold value. However, spontaneous generation of skyrmions does not occur due to the topological protection. Nevertheless, the topological protection can be violated in condensed matter physics because of the existence of the lattice structure and the boundary of the sample. We may create skyrmions by leveraging these properties.

Skyrmion Hall effect. It is well understood[22] that the center-of-mass motion of a skyrmion is determined by the Lagrangian,

$$L = L_B - U, \quad (4)$$

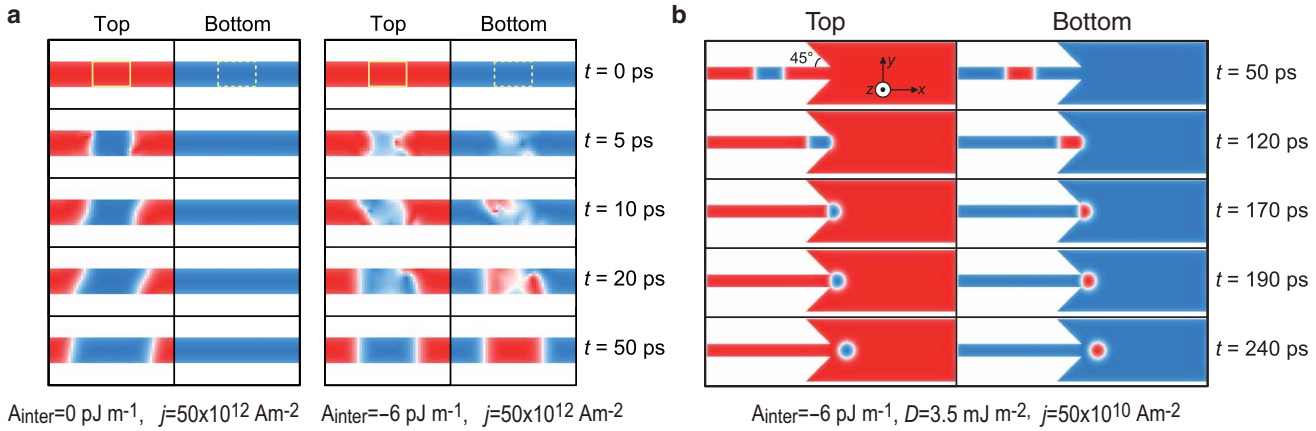

FIG. 3: **Creation of a bilayer DW pair, its conversion into a bilayer-skyrmion, and their motions driven by vertical current in a bilayer nanotrack.** The length, wide width and narrow width of the nanotrack (D = 3.5 mJ m^{-2}) equal 400 nm, 100 nm, and 20 nm, respectively. **a**, A local vertical spin current ($j = 50 \times 10^{12}$ A m^{-2}, $P = 0.4$, polarized along $-z$) is perpendicularly applied to the top layer of the narrow side (85 nm $< x <$ 115 nm) before t = 50 ps. When the top and bottom layers are decoupled ($A_{\rm inter}$ = 0 pJ m^{-1}), only one DW pair is generated in the top layer. However, when the top and bottom layers are coupled ($A_{\rm inter}$ = -6 pJ m^{-1}), a bilayer DW pair is created at t = 50 ps. **b**, A global vertical spin current is perpendicularly applied to the bottom layer (towards $+z$, polarized along $+y$) when the bilayer DW pair is created at t = 50 ps. The current density j in wide part equals 5×10^{11} A m^{-2}, which is proportional to that inside the narrow part with respect to the ratio of narrow proportion (200 nm $\times$ 20 nm) to wide proportion (200 nm $\times$ 100 nm). The 45-dgree notches are employed to reduce the required current density for the DW-skyrmion conversion. When the global driving current is turned on at t = 50 ps, the local DW injection current is turned off at the same time. See Supplementary Movie 3.

where L_B is the Berry phase term of the spin texture,

$$L_B = \frac{G}{2}(\dot{X}Y - X\dot{Y}) = \frac{1}{2}\boldsymbol{G}\cdot(\dot{\boldsymbol{R}}\times\boldsymbol{R}), \tag{5}$$

and U is the potential. Here, $\boldsymbol{G} = (0, 0, G)$ is the gyromagnetic coupling constant representing the Magnus force with $G = 4\pi Q$, and $\boldsymbol{R} = (X, Y)$ is the center-of-mass coordinate of the skyrmion. The Euler-Lagrange equation yields

$$\dot{\boldsymbol{R}} = \frac{1}{G}\boldsymbol{e}_z \times \boldsymbol{F}, \tag{6}$$

where $\boldsymbol{e}_z = (0, 0, 1)$, and $\boldsymbol{F} = -\nabla U$ is the force acting on the skyrmion. Consequently, a moving skyrmion feels the Magnus force and bends toward the direction perpendicular to the force. It is called the skyrmion Hall effect.

The direction of the Magnus force is opposite when the sign of the skyrmion number Q is opposite. For instance, if a skyrmion is driven by the current along the $+x$ direction it will be bended toward the $+y$ ($-y$) direction in the top (bottom) layer.

Landau-Lifshitz-Gilbert-Slonczewski equation for CPP

We may apply a CPP spin-polarized current injection from magnetic tunnel junction (MTJ) or the spin Hall effect in heavy metal layer[6,23,24]. We numerically solve the Landau-Lifshitz-Gilbert-Slonczewski (LLGS) equation, which governs the dynamics of the magnetization $\boldsymbol{m}_i$ at the lattice site i. By suppressing the layer index, it reads

$$\begin{aligned}\frac{d\boldsymbol{m}_i}{dt} =& -|\gamma|\boldsymbol{m}_i\times\boldsymbol{H}_i^{\rm eff} + \alpha\boldsymbol{m}_i\times\frac{d\boldsymbol{m}_i}{dt}\\ &+|\gamma|\,u(\boldsymbol{m}_i\times\boldsymbol{p}\times\boldsymbol{m}_i) - |\gamma|\,u'(\boldsymbol{m}_i\times\boldsymbol{p}),\end{aligned} \tag{7}$$

where $\boldsymbol{H}_i^{\rm eff} = -\partial H_{\rm total}/\partial\boldsymbol{m}_i$ is the effective magnetic field induced by the Hamiltonian $H_{\rm total} = H_{\rm T} + H_{\rm B} + H_{\rm inter}$, γ is the Gilbert gyromagnetic ratio, α is the Gilbert-damping coefficient originating from spin relaxation, u is the Slonczewski STT coefficient, u' is the out-of-plane STT coefficient, and $\boldsymbol{p}$ represents the electron polarization direction. Here, $u = |\frac{\hbar}{\mu_0 e}|\frac{j|\boldsymbol{p}|}{2dM_s}$ with μ_0 the vacuum magnetic permittivity, d the film thickness, M_s the saturation magnetization, and j the current density. We take $-z$ direction for creating the skyrmion, while $+y$ direction for moving the skyrmion. The STT is induced either by injection from a magnetic tunnel junction polarizer or by the spin Hall effect[6,23,24].

LLG equation for CIP

Alternatively we may apply a CIP injection[6,23,24] to move skyrmions. We numerically solve the LLG equation,

$$\begin{aligned}\frac{d\boldsymbol{m}_i}{dt} =& -|\gamma|\boldsymbol{m}_i\times\boldsymbol{H}_i^{\rm eff} + \alpha\boldsymbol{m}_i\times\frac{d\boldsymbol{m}_i}{dt}\\ &+\frac{\boldsymbol{p}|a^3}{2eM_s}(\boldsymbol{j}(\boldsymbol{r})\cdot\nabla)\boldsymbol{m}_i\\ &-\frac{\boldsymbol{p}|a^3\beta}{2eM_s}[\boldsymbol{m}_i\times(\boldsymbol{j}(\boldsymbol{r})\cdot\nabla)\boldsymbol{m}_i],\end{aligned} \tag{8}$$

where β is the strength of the non-adiabatic torque and a is the lattice constant.

Creation of a bilayer-skyrmion by vertical spin current. We employ a CPP injection with a circular geometry in a nanodisk. The spin-polarized current (polarized along $-z$) is injected into the top layer in the central circle region, as illustrated in Fig.1a.

We demonstrate how the spin textures develop in Fig.2a. The spins start to flip in both layers following the spin cur-

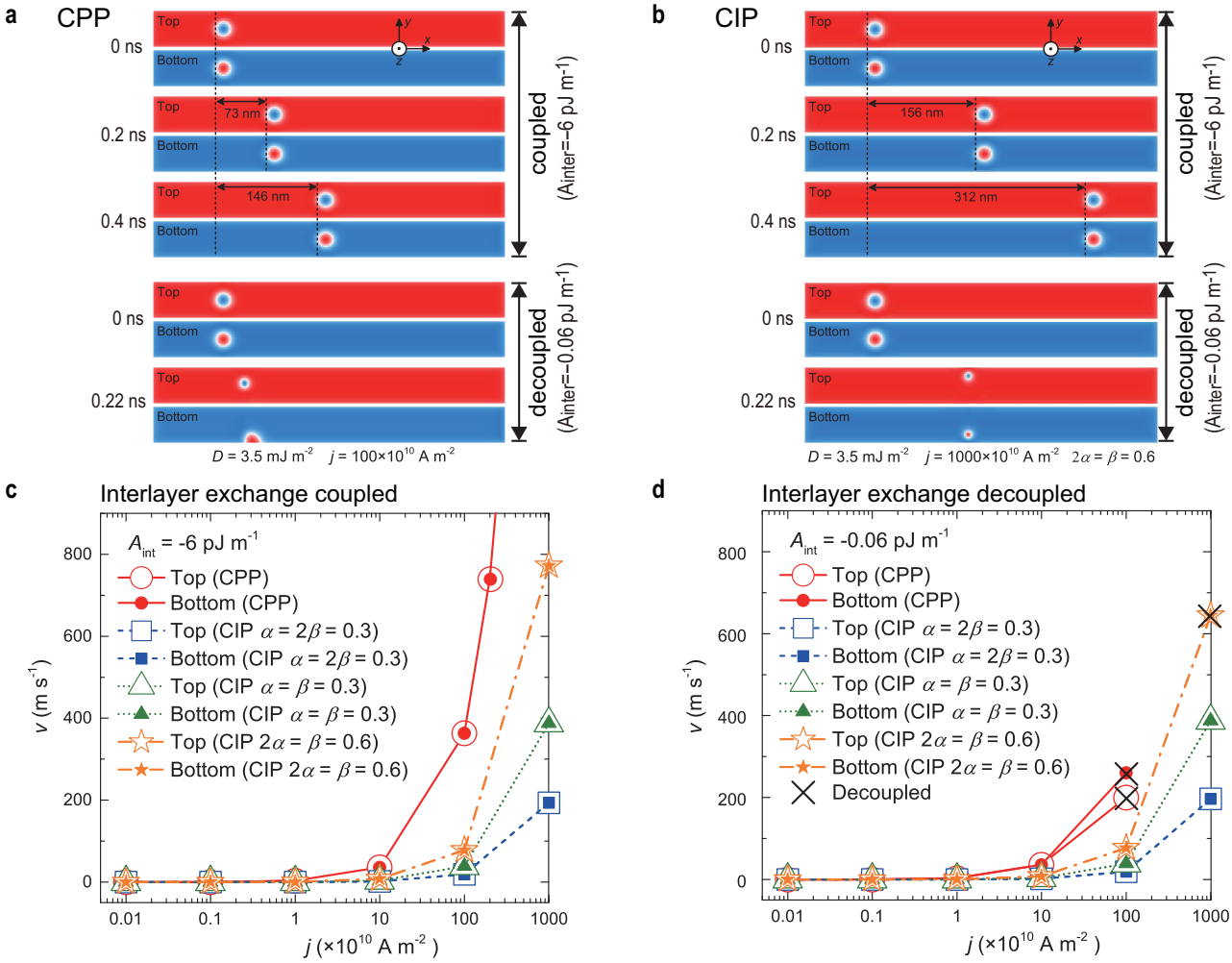

FIG. 4: **Motion of skyrmions in the top and bottom layers of a bilayer nanotrack.** Top-views of motion of skyrmions at selected interlayer exchange coupling and times driven by **(a)** the CPP injection and **(b)** the CIP injection (see Supplementary Movies 4-7). The parameters of the bilayer nanotrack are 500 nm × 50 nm × 3 nm, D = 3.5 mJ m^{-2}. The skyrmions are initially created by MTJ skyrmion injector placed on the top layer at x = 100 nm. For the CPP case, the spin current (P = 0.4) in the bottom layer is applied along $+z$ but polarized along $+y$. The skyrmion in the bottom layer moves towards right driven by the spin current, while the skyrmion in the top layer remotely moves due to the interlayer coupling. For the CIP case, the skyrmions in both the top and bottom layers are driven by in-plane spin currents (P = 0.4). The velocities of skyrmions in the top and bottom layers as functions of current density j with **(c)** large interlayer exchange A_{inter} = -6 pJ m^{-1} and **(d)** small interlayer exchange A_{inter} = -0.06 pJ m^{-1}. The cross symbol denotes the decoupling and destruction of skyrmions in the top and bottom layers due to large current density and small interlayer exchange coupling, where the velocities are calculated before the destruction of skyrmion.

rent injection only in the top layer. When there is no interlayer AFM coupling, a skyrmion is formed only in the top layer (see Supplementary Movie 1). By contrast, a skyrmion is formed also in the bottom layer upon the current injection in the presence of the interlayer AFM coupling (see Supplementary Movie 2).

We show the evolution of the skyrmion number in Fig.2b. It oscillates at the initial stage for $t < 0.2$ ns, and rapidly increases to 1. The skyrmion remains stable even when the current is switched off, demonstrating that it is topologically protected. During this process, the spins in the top and bottom layers are always anti-parallel. A comment is in order. The saturated skyrmion number is not exactly $Q = 1$ but $Q = 0.89$. This is due to the fact that there is a background skyrmion number which originates from the tilting the edge spins. It is $Q = -0.09$. Accordingly, the calibrated skyrmion number is $Q = 0.98$, which is almost unity.

We present a nucleation phase diagram of a bilayer-skyrmion pair as a function of the current density and the interlayer AFM coupling in Fig.2d and Fig.2e. When the magnitude of the injected current is strong enough, the bilayer-skyrmion is created. This is due to the fact that spin flip costs a certain energy. On the other hand, if the interlayer AFM coupling is too strong, the bilayer-skyrmion is suppressed due to the fact that the nucleation field and the coercivity increases with the interlayer AFM exchange, leading to a larger current

density for nucleation.

Creation of a bilayer-skyrmion from a bilayer DW pair. A magnetic skyrmion can be created from a DW pair by using a junction geometry[25]. In this scenario we first make a DW pair into a nanotrack of the top layer through the local CPP injection with $-z$ direction. We show how the spins start to flip in the top layer and subsequently in the bottom layer driven by the AFM exchange force in Fig.3a. Then, the bilayer DW pair is shifted by applying CPP current, as shown in the process from $t = 50$ ps to $t = 120$ ps in Fig.3b. Here we consider the vertical injection of a spin current towards $+z$ and polarized along $+y$ in the bottom layer. The CPP injection moves the bilayer DW in the rightward direction. When the bilayer DW arrives at the junction interface ($t = 170$ ps), both the end spins of the DW are pinned at the junction, whereas the central part of the DW continues to move due to STT in the wide part of the nanotrack. Therefore, the structure is deformed into a curved shape and a bilayer-skyrmion texture forms at $t = 190$ ps (see Supplementary Movie 3).

Current-driven motion of a bilayer-skyrmion in a nanotrack. The magnetic bilayer-skyrmion can be displaced by the vertical spin-polarized current as in the case of the magnetic skyrmion. We may employ the CPP injection or the CIP injection to drive a bilayer-skyrmion. In general, a moving skyrmion is easily destroyed by the sample edges due to the skyrmion Hall effect. Therefore, the maximum velocity of skyrmion in FM nanotrack is typically much less than 10^3 m/s, limited by the edge confining force[18] of $\sim D^2/J$.

The skyrmion in the top layer follows the motion of the skyrmion in the bottom layer even when the current is not injected into the top layer. This is because that two skyrmions are bounded by the interlayer AFM coupling. There is no skyrmion Hall effect for a magnetic bilayer-skyrmion. This can be explained as follows. If there is no interlayer AFM coupling, a skyrmion in the top layer moves left-handed and the skyrmion in the bottom layer moves right-handed. However, when the AFM coupling is strong enough, two skyrmions are tightly bounded and the Magnus forces acting on the skyrmions between the top and bottom layers are exactly cancelled. Accordingly the bilayer-skyrmion will move straightly. This mechanism works both for the CPP and CIP cases (see Supplementary Movies 4-5).

We show the relation between the magnitude of the injected current and the velocity in Fig.4. The velocity is proportional to the injected current density. For strong enough current, the bilayer-skyrmion is destroyed and split into two independent skyrmions. This is because that the skyrmion Hall effect increases as the current increases, which acts as the repulsive force between two skyrmions (see Supplementary Movies 6-7).

With strong interlayer AFM exchange coupling, the coupled skyrmions move along the central line of the nanotrack at a high speed of a few hundred meters per second, without any transverse motion. However, with small interlayer AFM exchange coupling, the skyrmions in the top and bottom layers will be decoupled due to the fast motion of the skyrmion in the bottom layer driven by large current. Once the skyrmions in the top and bottom layers are decoupled, the skyrmion Hall effect becomes active, leading to the destruction of skyrmions in the top and/or bottom layer by touching edge. At the same time, in the CPP case, the skyrmion in the top layer will stop motion. It can be seen that the coupled skyrmions driven by CIP current doesn't require a fine tuning of damping and non-adiabatic torque coefficients.

It is also worth noting that the interlayer AFM coupling does not produce a mass of the bilayer-skyrmion. When the driving current is suddenly turned off, the bilayer-skyrmion stops high-speed motion immediately (see Supplementary Movie 8). On the other hand, we also investigated the case where the DMI constant D is different between the top and bottom layers. It is found that the results of current-driven motion of the bilayer-skyrmion do not change much since the DMI only changes the radius of the skyrmion (see Supplementary Movies 9-10). The massless property and its robustness make the bilayer-skyrmion an ideal candidate for practical applications.

Perspectives

We have presented a novel solution of inhibiting the Hall effect of skyrmions without affecting their topological properties, by exploring a new device made of antiferromagnetically exchange-coupled bilayer nanodisks and nanotracks. Compared with the mostly investigated skyrmion in the FM monolayer system, the bilayer-skyrmion exhibits entirely distinct characteristics with regard to the current-transport behaviour and robustness. First, it can move strictly along the direction of the spin current flow, which makes it more appealing for motions in nanowires for ultradense memory applications. This is in high contrast with the case of monolayer skyrmion, where the skyrmion information carrier can be easily destroyed by the edges of the nanotracks. Second, it will be immune to magnetic field perturbations which might be generated externally or internally within the device circuitry since the net magnetic moment is zero. Third, by introducing the bilayer degree of freedom, the transport properties of the device can be engineered to achieve desired performance. For example, the skyrmion Hall effect can be intentionally suppressed or enhanced by tuning the magnetic properties of individual layers. This newly proposed solution of transporting skyrmion information carrier for arbitrarily long distances at much enhanced velocity may be very appealing for versatile applications such as ultradense memory and information processing. Similar ideas can be extended to multilayer or superlattice where the skyrmions are strongly coupled to realize a better manipulation of skyrmions in nanotrack or extended thin films.

Methods

Modeling and simulation. The micromagnetic simulations are performed using the Object Oriented MicroMagnetic Framework (OOMMF) including the Dzyaloshinskii-Moriya interaction (DMI) extended module[5,6,26,27]. The time-dependent magnetization dynamics is governed by the Landau-Lifshitz-Gilbert (LLG) equation including spin torque[28–32]. The average energy density E is a function of $\mathbf{M}$, which contains the intralayer exchange, the interlayer exchange, the anisotropy, the applied field (Zeeman), the demag-

netization and the DMI energy terms. For micromagnetic simulations, the intrinsic magnetic parameters are adopted from Refs.[5,6]: Gilbert damping coefficient $\alpha = 0.3$ and the value for Gilbert gyromagnetic ratio is -2.211$\times$ 10^5 m A^{-1} s^{-1}. Saturation magnetization M_S = 580 kA m^{-1}, intralayer exchange stiffness A = 15 pJ m^{-1}, DMI constant $D = 0 \sim 6$ mJ m^{-2} and perpendicular magnetic anisotropy (PMA) K = 0.8 MJ m^{-3} unless otherwise specified. The interlayer exchange coefficient A_{inter} is set from 0 to -10 pJ m^{-1}, whereas the corresponding interface exchange coefficient σ equals from 0 to -10 mJ m^{-2} (σ = A_{inter} / 1 nm), where "-" denotes that the interface is antiferromagnetically coupled. The field-like out-of-plane STT coefficient u' is set to zero. All samples are discretized into cells of 2 nm $\times$ 2 nm $\times$ 1 nm in the simulation, which is sufficiently smaller than the typical exchange length ($\sim$ 4.3 nm) and the skyrmion size to ensure the numerical accuracy. For all simulation of current-driven skyrmions reported throughout this paper, the skyrmions are firstly created at the designed spot of the nanotrack (x = 100 nm) by a local spin current perpendicular to the plane of the top layer. Then the system is relaxed to an energy minimum state without applying any current. Next, we start the timer and the spin current (P = 0.4) is injected into the nanotrack with the geometry of current-in-plane (CIP) or current-out-of-plane (CPP) as shown in Fig.1. In the configuration of CIP, the electrons flow toward the right in both the top and bottom layers, $i.e.$, the currents flow toward the left, while in the configuration of CPP, the electrons flow toward the top only in the bottom layer.

* Corresponding author: yanzhou@hku.hk
† Corresponding author: ezawa@ap.t.u-tokyo.ac.jp

1 S. Mhlbauer et. al. Science **323**, 915 (2009).
2 X. Z. Yu et. al. Nature **465**, 901 (2010).
3 S. Heinze et. al. Nature Phys. **7**, 713 (2011).
4 N. Nagaosa and Y. Tokura, Nat. Nanotech. **8**, 899 (2013).
5 A. Fert, V. Cros, and J. Sampaio, Nat. Nanotech. **8**, 152 (2013).
6 J. Sampaio, V. Cros, S. Rohart, A. Thiaville, and A. Fert, Nat. Nanotech. **8**, 839 (2013).
7 Y. Tchoe and J. H. Han, Phys. Rev. B **85**, 174416 (2012).
8 Y. Zhou, E. Iacocca, A. Awad, R. K. Dumas, F. C. Zhang, H. B. Braun, and J. Akerman, cond-mat/arXiv:1404.3281.
9 M. Finazzi, M. Savoini, A. R. Khorsand, A. Tsukamoto, A. Itoh, L. Duo, A. Kirilyuk, Th. Rasing, and M. Ezawa, Phys. Rev. Lett. **110**, 177205 (2013).
10 X. C. Zhang, M. Ezawa, and Y. Zhou, Sci. Rep. **5**, 9400 (2015).
11 X. C. Zhang, G. P. Zhao, H. Fangohr, J. P. Liu, W. X. Xia, J. Xia, and F. J. Morvan, Sci. Rep. **5**, 7643 (2015).
12 C. Moreau-Luchaire, C. Moutafis, N. Reyren, J. Sampaio, N. Van Horne, C.A.F. Vaz, K. Bouzehouane, K. Garcia, C. Deranlot, P. Warnicke, P. Wohlhüter, J.M. George, J. Raabe, V. Cros, and A. Fert, arXiv:1502.07853 (2015).
13 S. Woo, K. Litzius, B. Krüger, M. Y. Im, L. Caretta, K. Richter, M. Mann, A. Krone, R. Reeve, M. Weigand, P. Agrawal, P. Fischer, M. Kläui, G. S. D. Beach, arXiv:1502.07376 (2015).
14 S. Parkin, and S. Yang, Nat. Nanotech. **10**, 195 (2015).
15 N. Bogdanov and D. A. Yablonskii, Sov. Phys. JETP **68**, 101 (1989).
16 N. Bogdanov and A. J. Hubert, Magn. Magn. Mater. **138**, 255 (1994).
17 U. K. Roessler, N. Bogdanov, and C. Pfleiderer, Nature **442**, 797 (2006).
18 J. Iwasaki, W. Koshibae, and N. Nagaosa, Nano Lett., **14**, 4432 (2014).
19 J. Iwasaki, M. Mochizuki, and N. Nagaosa, Nat. Nanotech. **8**, 742 (2013).
20 J. Iwasaki, M. Mochizuki, and N. Nagaosa, Nat. Commun. **4**, 1463 (2012).
21 S. H. Yang, K. S. Ryu, and S. Parkin, Nat. Nanotech. **10**, 221 (2015).
22 M. Stone, Phys. Rev. B **53**, 16573 (1996).
23 A.V. Khvalkovskiy, V. Cros, D. Apalkov, V. Nikitin, M. Krounbi, K.A. Zvezdin, A. Anane, J. Grollier, and A. Fert, Phys. Rev. B **87**, 020402(R) (2013).
24 R. Tomasello, E. Martinez, R. Zivieri, L. Torres, M. Carpentieri, and G. Finocchio, Sci. Rep. **4**, 6784 (2014).
25 Y. Zhou and M. Ezawa, Nat. Com. **5**, 4652 (2014).
26 M. J. Donahue and D. G. Porter, National Institute of Standards and Technology, Interagency Report NISTIR, **6376** (1999 OOMMF user's guide, version 1.0.).
27 S. Rohart and A. Thiaville, Phys. Rev. B **88**, 184422 (2013).
28 W. F. Brown J., Micromagnetics (Krieger, New York, 1978).
29 T. L. Gilbert, Phys. Rev. **100**, 1243 (1955).
30 L. Landau and E. Lifshitz, Physik. Z. Sowjetunion **8**, 153 (1935).
31 A. Thiaville, S. Rohart, E. Jue, V. Cros, and A. Fert, Europhys. Lett. **100**, 57002 (2012).
32 A. Thiaville, Y. Nakatani, J. Miltat, and Y. Suzuki, Europhys. Lett. **69**, 990 (2005).

Acknowledgements

Y.Z. thanks the support by the Seed Funding Program for Basic Research and Seed Funding Program for Applied Research from the HKU, ITF Tier 3 funding (ITS/171/13), the RGC-GRF under Grant HKU 17210014, and University Grants Committee of Hong Kong (Contract No. AoE/P-04/08). M.E. thanks the support by the Grants-in-Aid for Scientific Research from the Ministry of Education, Science, Sports and Culture, No. 25400317. M.E. is very much grateful to N. Nagaosa for many helpful discussions on the subject.

Author contributions

M.E. conceived the idea and designed the project. M.E. and Y.Z. coordinated the project. X.Z. performed the numerical simulations supervised by Y.Z. All authors discussed the results and wrote the manuscript.

Additional information

Supplementary information is available.

Competing financial interests

The authors declare no competing financial interests.